COMPASsCO$_2$

COMPONENTS' AND MATERIALS' PERFORMANCE FOR ADVANCED SOLAR SUPERCRITICAL CO2 POWERPLANTS

# Demonstration of New Cr aluminides and production of coupons for WP4 testing

**Deliverable Number:** 3.1

**WP3:** Development of Materials

**Date**: November 3rd, 2022

**Deliverable type**: Report

**Dissemination level**: Public

**Lead participant**: University of Birmingham

This project has received funding from the European Union's Horizon 2020 Research and Innovation Action (RIA) under grant agreement No. **958418.**

## AUTHORS


| Name | Organisation |
|---|---|
| Tom Blackburn, Dr Kan Ma, Dr Sandy Knowles | UoB |
| Michael Kerbstadt, Dr Mathias Galetz | DFI |
| Dr Tatu Pinomaa | VTT |
| Dr Hernandez Pascual Rebeca, Dr Marta Serrano | CIEMAT |
| Dr Krista Van den Bergh | OCAS |


## DOCUMENT HISTORY

| Version | Date | Change |
|---|---|---|
| 01 | 03.11.2022 | Initial version |
| | | |

## ABOUT THE PROJECT

COMPASsCO$_2$ is a 4-year HORIZON2020 project started on 1.11.2020. It is led by the German Aerospace Centre (DLR), with eleven additional partners from seven European countries.

COMPASsCO$_2$ aims to integrate CSP particle systems into highly efficient s-CO$_2$ Brayton power cycles for electricity production. In COMPASsCO$_2$, the key component for such an integration, i.e. the particle/s-CO$_2$ heat exchanger, will be validated in a relevant environment. To reach this goal, the consortium will produce tailored particle and alloy combinations that meet the extreme operating conditions in terms of temperature, pressure, abrasion and hot oxidation/carburisation of the heat exchanger tubes and the particles moving around/across them. The proposed innovative CSP s-CO$_2$ Brayton cycle plants will be flexible, highly efficient, economic and 100% carbon neutral large-scale electricity producers.

The research focus of COMPASsCO$_2$ is on three main technological improvements: development of new particles, development of new metal alloys and development of the heat exchanger section.

## DISCLAIMER

This project has received funding from the European Union's Horizon 2020 Research and Innovation Action (RIA) under grant agreement No. **958418.**

# TABLE OF CONTENTS

# LIST OF FIGURES

# LIST OF TABLES



# LIST OF ABBREVIATIONS

| | |
|---|---|
| COMPASsCO$_2$ | Components' and Materials' Performance for Advanced Solar Supercritical $CO_2$ Power Plants |
| CST | Concentrating Solar Thermal |
| CSP | Concentrated Solar Power |
| EC | European Commission |
| EU | European Union |
| UoB | University of Birmingham |
| CSP | Concentrated Solar Power |
| sCO$_2$ | Supercritical $CO_2$ |
| BCC | Body Centered Cubic |
| $T_m$ | Melting Point |
| DBTT | Ductile to Brittle Transition Temperature |
| PVs | Solar Photovoltaics |
| CALPHAD | CALculation of PHAse Diagram |
| SEM | Scanning Electron Microscope |
| TEM | Transition Electron Microscope |
| STEM | Scanning Transition Electron Microscope |
| EDX | Energy Dispersive X-rays |
| XRD | X-Ray Diffraction |
| FIB | Focused Ion Beam |
| APT | Atom Probe Tomography |
| SPT | Small Punch Testing |
| EBSD | Electron BackScatter Detection |

# 1 ABSTRACT

Work Package 3 of the H2020 COMPASsCO2 project is focussed on 'Development of metals' bringing together partners from University of Birmingham, CIEMAT Madrid, DFI Dechema Frankfurt, OCAS Belgium, VTT Finland.

Chromium-based superalloys are a desirable candidate material for the heat exchanger in the next generation of concentrated solar power (CSP) owing to their high melting points, excellent corrosion properties and low cost compared to austenitic steels and nickel superalloys. However, improvements in their mechanical properties is critical for their engineering application. A 'bcc-superalloy' approach utilising a bcc chromium matrix strengthened by ordered bcc-nickel aluminide precipitates is under development. Alloy designs were instructed by a CALPHAD approach. Samples were arc melted, followed with homogenisation and aging by heat treatment to create the target microstructure and control precipitate volume fraction. Chromium alloys appear to bear greater thermal stability over alternative high temperature materials such as nickel superalloys, cobalt superalloys and ferritic superalloys. Additionally, iron additions increase the hardness or the alloys and reduce age softening over their ternary alloy equivalent. Preliminary oxidation results show improved oxidation resistance of these alloys. Following on from this report, material production of coupons for WP4 will commence in accordance with the sample geometries and quantities required by each partner. Upon providing the required coupons, an updated report will be published.

# 2 INTRODUCTION

The design of a heat exchanger to operate at high temperature (>700$^{o}$C), high pressure (>25 MPa), corrosive and high wear environment presents significant challenges for current state-of-the-art advanced austenitic stainless steels and nickel superalloys (Ni-superalloys). Refractory Body Centred Cubic (BCC) metals on the other hand, such as chromium, present highly desirable characteristics for such applications owing to their higher melting points ($T_m$), low cost, lower mass density, good thermal conductivity and high temperature oxidation resistance. However, as with all BCC metals they exhibit a Ductile to Brittle Transition Temperature (DBTT, typically around 0.15 $T_m$) meaning they are typically brittle at room temperature which has hindered their engineering adoption to date (1,2).

While significant investigations were carried out in the 1950s and 60s into the binary additions of chromium namely for the aerospace industry, increased attention into nickel-based superalloys and the drawbacks of refractory bcc alloys lead to the demise of scientific interest into such alloys until recently. This project focuses on the development of β-β' BCC superalloy incorporating a disordered-BCC A2 (β) chromium matrix and ordered-BCC B2 (β') nickelaluminide (NiAl) intermetallic precipitates which also have a high $T_m$, low density, good oxidation resistance, and low lattice misfit (3,4). The high temperature strength of an alloy can be developed significantly by solid solution strengthening but will co-inside with a reduction in ductility, here precipitation hardening can achieve a similar result with a lesser effect on the ductility of the alloy (2).

This report presents the initial work during the first stage of Task 3.1 in this project, focusing on the Cr-NiAl and Cr-NiAl-(Fe) alloys. The report will present an introduction to Cr-NiAl alloys followed by a review of Cr-NiAl alloys. Then experiments, results and conclusions will be presented with a plan of work to be carried out.

# 3 BACKGROUND

## 3.1 APPLICATION BACKGROUND

The need for short and long term (to counter day-night and seasonal fluctuations in demand and production) electricity storage has been identified as a crucial step if we are to transfer from fossil fuels to a green electricity grid (5). One potential solution is Concentrated Solar Power (CSP) where sunlight is reflected from an array of heliostats (auto-positioning mirrors) to a central point where a medium is heated which then is passed through a steam generator to generate electricity. Current designs, namely the power tower type, are currently limited by lower thermal efficiencies driven by low operating temperatures (<550$^{o}$C (6)).

The next generation CSP (Figure 1) is seeking to increase the maximum operating temperature to >700$^{o}$C to utilise the greater thermal efficiencies offered by the supercritical $CO_2$ ($sCO_2$) Brayton Cycle (due to the high density and low viscosity of $sCO_2$ (7)). The system will use novel solid ceramic particles (developed by Saint-Gobain) as the primary heated medium allowing ease of energy storage via the thermal storage of the heated particles allowing power production 24 hours a day. Thermal storage like this offers a cheaper form of energy storage than lithium-ion battery storage in a far more stable and simple manner. Significant challenges are thus presented with the high temperature (>750$^{o}$C), high pressure (>25 MPa), corrosive and high wear environment within the heat exchanger.

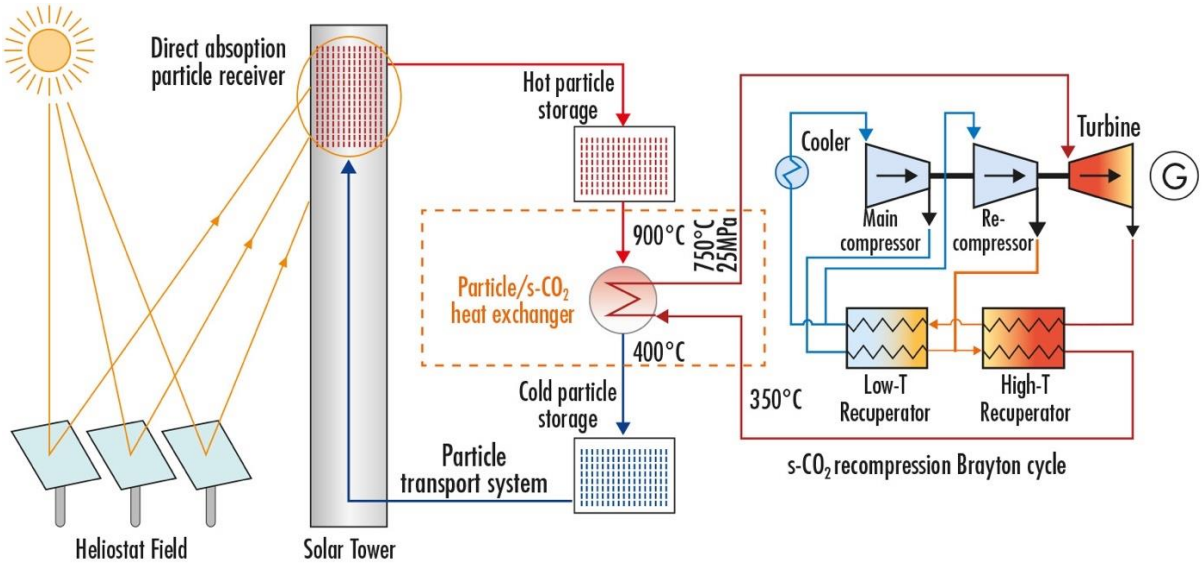


*Figure 1: Schematic illustration of a CSP plant indicating the main components and power generation cycle (https://www.compassco2.eu).*

While some advanced austenitic stainless steels (e.g. Sanicro 25) and Ni-superalloys (e.g. Haynes 825) are being considered, a further increase in service temperature is limited by their strength at high temperatures particularly (~1200$^{o}$C (8)). Refractory BCC metals on the other hand, like chromium-based alloys, present highly desirable characteristics for such applications owing to their higher $T_m$, low cost, lower mass density (Table 1) and high temperature oxidation resistance. However, pure chromium lacks strength and creep resistance (9). Moreover, as with all BCC metals, they exhibit a Ductile to Brittle Transition Temperature (DBTT, typically around 0.15 $T_m$) meaning they are usually brittle at room temperature which has hindered their engineering adoption to date (1,2). Therefore, the strengthening and ductilisation of chromium alloys is crucial to their application.

*Table 1: Density and melting point ($T_m$) of elements and Ni-superalloy CMSX-4*

| Element | Density (g cm$^{-3}$) | Melting Point ($^o$C) | Thermal conductivity (W/m K) |
|---|---|---|---|
| Cr | 7.14 (8,10) | 1890 (8,11,12) | 93.7 (13) |
| Ni | 8.9 (2) | 1453 (14) | 90.7 (13) |
| Al | 2.7 (15) | 660 (14) | 237 (13) |
| Fe | 7.87 (15) | 1535 (14) | 80.2 (13) |
| Co | 8.85 (12) | 1495 (14) | 99.2 (13) |
| CMSX-4 | 8.7(16) | 1396 (17) | 10 (18) |

## 3.2 SOLID-SOLUTION STRENGTHENING AND DUCTILISATION OF CHROMIUM

The DBTT of pure chromium varies from -196$^o$C to 170$^o$C, which was reported to depend strongly on its purity (12). Namely nitrogen impurities which at levels >30ppm is said to cause embrittlement. However, it is mostly accepted that pure Cr is brittle at room temperature (19–21). During the 1950s and 60s extensive research was conducted into binary additions (Figure 2) to chromium in the pursuit of improved ductility at room temperature. However, a drawback of much of the research conducted in the 50s and 60s was that they utilised iodide chromium as this was the purest form of chromium available at the time. Advancements in production has meant that nowadays higher purity chromium is readily attainable meaning that much of the prior research pre-millennium can't be accurately comparable.

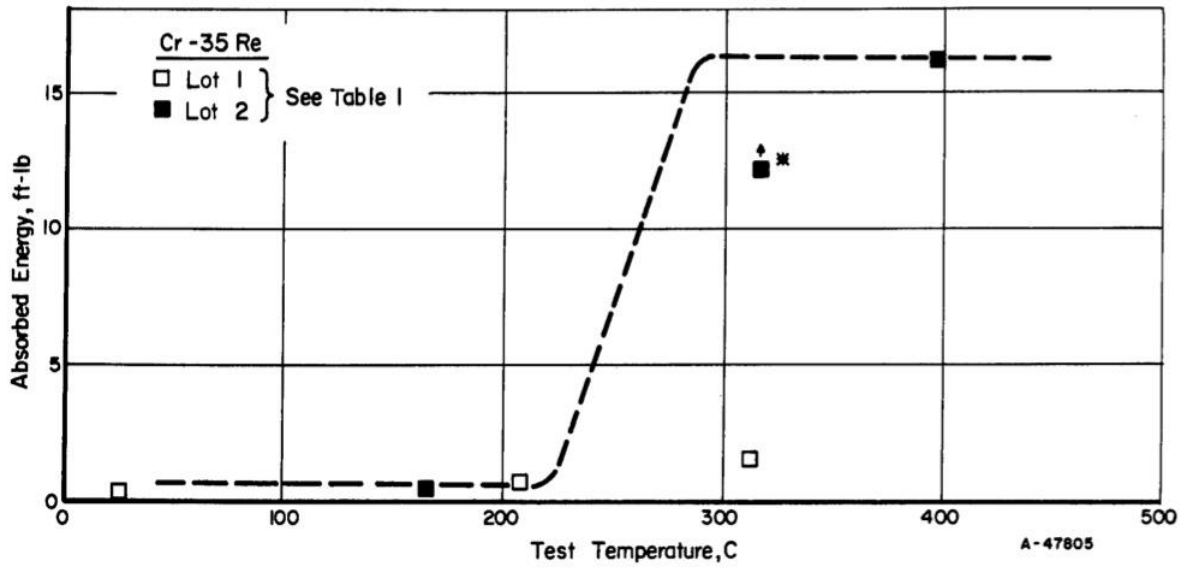


*Figure 2: DBTT of a Cr-35Re alloy form Gilbert, 1964 indicating the upper shelf (ductile) region and lower shelf (brittle region) with a transition temperature in between (22).*

## 3.3 RHENIUM DUCTILISING EFFECT

Rhenium, as a known ductiliser of chromium but high cost has resulted in much research to find analogs that are more cost effective and abundant yet still offer the ductilising effect. In a NASA investigation by Klopp, 1969, ruthenium, iron, osmium, cobalt and manganese were identified as potential rhenium analogs (2). This was confirmed in their later study that furthered their conclusion that cobalt and iron alloys need to be quenched to exhibit the twinning that is observed in rhenium alloys (23). In general, alloying additions from groups 7b and 8b from the periodic table are thought to be ductilising metals (24).

## 3.4 CHROMIUM-IRON

Iron, being less dense than other Re-ductilising analogs and Ni-superalloys (Table 1), has been found to increase the grain size of chromium alloys (1,25). Particularly at high temperatures (>1000$^{o}$C) Cr-40Fe has been found to have increased strength over Ni-superalloys (26). Moreover, the high temperature properties of this alloy were investigated by Ro, 2002 who found it to have a tensile stress of 120 MPa at 1200$^{o}$C and 90 MPa at 1300$^{o}$C (8). Furthermore, a Cr-50Fe was found by Abiko, 1998 to have a yield stress of 550 MPa and a tensile stress of 680 MPa at room temperature (27). However, Cr-Fe has been noted to have a low ductility due to deformation hardening (28).

## 3.5 OTHER ALLOYING ADDITIONS

Cerium and zirconium are also thought to improve the room temperature ductility of chromium (24). In the research by Gu, 2004, they found that tantalum and niobium could be ductilising elements, but the results are erratic. They also presented conflicting evidence that titanium, vanadium and molybdenum alloys were un-fabricable while other investigations specifically into molybdenum additions were able to produce and investigate such alloys (19,29). Research into molybdenum additions to chromium is more extensive yet still limited than other alloying additions. Molybdenum was found to improve coarsening rates in Cr-CrSi alloys which may also be synonymous to other β/β' alloys (30). In the investigation by Vo, 2014, molybdenum was found to increase ductility by increasing grain boundary cohesion as the grain boundary is thought to be sites of crack initiation (29). Moreover, molybdenum is thought to increase the surface energy of chromium hence improving ductility (19). As well as molybdenum, niobium and vanadium are also considered as β, stabilisers (3). Cr-Co has been identified as unsuitable for high temperature applications due to the formation of $\sigma$ phase during slow cooling (1). Small additions of vanadium have been found to improve the ductility of chromium however in the same investigation they found that too much vanadium can have the inverse effect on the ductility of chromium (19). Rather pessimistically, research conducted by Klopp, 1975 concluded that chromium, molybdenum and tungsten alloys that intend to be used at high temperature must be coated for corrosion resistance (23).

## 3.6 'BCC-SUPERALLOY' STRENGTHENING OF CHROMIUM

Inspired by the γ/γ' microstructure of Ni-superalloys, β/β' BCC-superalloy are in development, which incorporates an A2 (β) chromium matrix and ordered BCC B2 (β'), such as nickelaluminide (NiAl), intermetallic precipitate which also has a high $T_m$, low density, good oxidation resistance, and low lattice misfit (3,4). The high temperature strength of an alloy can be developed significantly by solid solution strengthening but will co-inside with a reduction in

ductility, here precipitation hardening can achieve a similar result with a lesser effect on the ductility of the alloy (2). The extent of the strengthening by precipitation is governed by the Orowan coarsening equation 1:

$$\sigma = \sigma_0 + C' \frac{f^{0.5}}{d} \quad (1)$$

where σ, is the yield strength (MPa), $\sigma_0$ is the matrix strength (MPa), f is the volume fraction of the precipitate and d is the particle diameter (nm).

Due to the requirement of precipitates in BCC superalloys, coarsening rates must be considered and in order to deduce any improvements of chromium alloys over conventional Fe and Ni-superalloys comparisons must be made to their own coarsening rates (31–36).

It can be identified that Ni-superalloys have a greater coarsening rate at higher temperatures over Fe-superalloys. Further investigation will be required to deduce the diffusion coefficients in order to make predictions of the coarsening rate of nickel and aluminium in a chromium matrix.

While Cr-superalloys have not been the subject of extensive research recently, the Cr-Ni-Al ternary system has. This is largely due to the development of Ni-superalloys for the aerospace industry hence, the majority of research to date exists in the nickel rich region of the ternary system. When comparing the lattice parameters (Table 2), it can be seen that the lattice parameters for chromium, iron and NiAl are very similar as also found by Naka, 2002 (4).

*Table 2: Lattice parameters for chromium, iron, nickel, aluminium, and their precipitates.*

| Crystal | Lattice Parameter Å |
|---|---|
| Cr | 2.8848 (37) |
| NiAl | 2.886-2.888 (4,29,38,39) |
| Ni2AlTi | 2.850 (38) |
| Fe | 2.872 (40) |
| Al | 4.0496 (37) |
| Ni | 3.510 (40) |

The investigation by Ferreriros, 2017 also found this to be the case for iron and NiAl which lead to a coherent precipitate within the iron matrix (34). Therefore, it was postulated that a similar result can be achieved with a chromium matrix. The NiAl phase will contribute to precipitate strengthening of the alloy. However, a potential drawback of Cr-NiAl alloys is the low solubility of NiAl in the chromium matrix which is thought to be around 14 at.% (41). In the study by Dogan, 2013, the temperature at which NiAl precipitates begin to form is 1345°C while the Ni2AlTi phase forms below 1130°C and in order to produce coherent, spherical eutectic precipitates, fast cooling (i.e. quenching) must occur (39,41). Numerous studies (38,39) have suggested different precipitate sizes based on different heat treatments, yet the coarsening rate of the NiAl phase within a chromium matrix has yet to be documented and especially not with the effect of different alloying additions. Coarsening rate was however investigated by Ferreriros, 2017, into the Fe-NiAl system which went further into the coarsening mechanisms using the critically resolved shear stress to determine the active mechanisms (34). Their study

also identified that the NiAl phase sheared on the <111> plane which should be broadly the same for the Cr-NiAl system but is yet to be confirmed. Dogan's study, 2013, identified that precipitates preferentially formed on grain boundaries leaving the region around the grain boundary free of solute and precipitates (39). In the same study they also identified that after ageing at 1000ºC the alloy contains both coarse (200-500 nm diameter) and fine precipitates (30-70 nm diameter) suggesting that even the fastest cooling rate possible can't prevent the nucleation of new precipitates upon cooling. Similar results were also identified in the study by Magnussen, 2019, who also confirmed the maximum solubility limit was between 10 and 20 at.% for the NiAl phase since a Cr-5Ni-5Al alloy would be fully homogenised after heat treatment at 1400ºC for 20 hr while a Cr-10Ni-10Al alloy could not be homogenised and instead was left with dendritic NiAl (42). Their work also provided an initial in-site to the micro-mechanics of Cr-NiAl alloys identifying dislocation slip to occur on the <111> and 100 planes in the NiAl phase while occurring on the <100>, <111>, and <112> planes in the chromium matrix. However, they identified that the active slip systems change depending on exact composition of the alloy where much work still remains.

One limiting factor for the implementation of chromium is its poor creep resistance at high temperature. Here, additions of the NiAl phase can improve the creep performance by providing more barriers for dislocation movement (41). Small additions of molybdenum was found by Vo, 2014, to reduce the coarsening of the NiAl phase and improve the creep properties (29). While this study focused on the Fe-NiAl system, it is thought that similar effects could be seen in the Cr-NiAl system. Initial investigations into Cr-NiAl systems focus on equiatomic NiAl but the investigation by Royer, 2008, concluded that increasing the ratio between nickel and aluminium resulted in an increased hardness of the annealed alloy (41).

The addition of titanium to a NiAl containing alloy (producing Ni2AlTi) can strengthen the NiAl particularly at higher temperatures as these two phases share a cube-cube orientational relationship (3). However, additions of titanium exceeding 10 at.% can lead to the undesirable formation of the laves phase (43).

## 3.7 MECHANICAL PROPERTIES

Hardness of Cr-50Ni was studied by Asahina, 2000, who found that it could be increased by additions of aluminium yet failed to identify that these additions produced the NiAl phase (44). The study by Maykuth, 1966, concluded that the strength of precipitate strengthened alloys depends on the distribution and size of the precipitate meaning the coarsening rate is an important parameter to investigate in such alloys (12). Their study also identified the hardness of pure chromium to be between 120 and 300 HV although acknowledged the difficulty of purifying chromium leads to inconsistent results due to strong effect of impurities to the properties of chromium (12). Hardness and yield stress of chromium based alloys have been extensively studied by NASA as well as others and results can be found in their papers (1,12,45–47). In summary however, alloying additions almost always increase the hardness of pure chromium; with ruthenium, iron and niobium being notable hardening additions. Despite this, some additions like iron appear to exhibit a maximum hardness which is yet to be identified accurately. An increased hardness has been correlated by Filippi, 1970, to a high DBTT (48). Therefore, alloy design must account for both high temperature strength as well as the desire for ductility.

The change in strength of pure chromium with increased temperature was studied by Gu, 2004 and identified that at room temperature chromium has a compressive yield stress of 200 MPa

at 1200ºC and 70 MPa (24). While Naka, 2002 commented on the yield stress of the NiAl phase to be between 100-200 MPa, Vo, 2014 commented on the shear stress required to cut the NiAl precipitates to be 920 MPa (3,4,29). Numerous researchers have attempted to identify the reason behind chromium's inherent brittleness all which seem to point towards the number of active slip systems or the lack of that make chromium brittle (42). Since chromium only has 3 active systems at room temperature while 5 are needed form room temperature ductility (49). Alternatively, Lu, 2021 suggested that it is the ratio of velocity between edge and screw dislocations that is the controlling factor in the DBTT of chromium (50). While Matsumoto, 2004, proposes that it is due to the low surface energy of chromium (19).

Regarding the creep properties of chromium alloys, Locq, 2011 studied the creep of quaternary titanium containing alloys at 1100ºC and concluded alloys containing 4 at.% titanium exhibited a lower creep rate than alloys containing 8 at.% titanium which was thought to be due to the hardening effect on the NiAl precipitates. Additionally, the incorporation of NiAl precipitates reduced the creep rate by a factor of 100 over pure chromium alloys however creep rates in these alloys were still greater than those in the Cr-CrSi system (38). Although creep has been studied in the quaternary system, it is yet to be studied in the ternary Cr-NiAl system nor has a detailed investigation into the 4 mechanisms involved in the Mukerjee-bird-dorn creep equation been investigated as proposed by Vo, 2014 (29).

## 3.8 AIMS AND OBJECTIVES

To sum up, the objective in the initial stage of this work is to:

- Demonstrate the alloy design in Cr-NiAl alloys with Fe addition to enhance precipitate volume fraction;
- Determine microstructure stability which corresponds to the coarsening rate of the NiAl precipitate of Cr superalloys;
- Investigate the mechanical properties of Cr-superalloys at room temperature.

# 4 EXPERIMENTAL TECHNIQUES AND METHODOLOGY

## 4.1 PHASE DIAGRAM CALCULATION

CALculation of PHAse Diagram (CALPHAD) was employed for initial composition selection. The ternary phase diagram of Cr-Ni-Al was analysed at 1200ºC and 1400ºC under atmospheric pressure using the TCNI-8 database.

Pseudo-binary Cr-NiAl(-Fe) was investigated while fixing the amount of Fe in the system to ensure the ageing temperature would remain in a single-phase region.

Caution must still be taken when reading into CALPHAD results since limited data is available for chromium-based alloys. While TCNI-5 and TCNI-8 databases produced exactly the same results, it was decided to utilise TCNI-8 (as was also used in Pfizenmaier's study (47)) as it allowed more variety for future alloying additions.

## 4.2 ARC MELTING

Compositions were first weighed out from pure element granules or wires (>99.9% purity) from various suppliers (American Elements, Keyue and Alfa Aesar) on a high precision mass balance. From experience (and the study by Pfizenmaier (47)) approximately 1 at.% extra chromium must be added to compensate for its high volatility during the casting process. Compositions were placed into a water-cooled copper hearth (Figure 3) alongside a titanium getter before the chamber was back filled and purged with argon three times and finally returned to 760 mmHg pressure during the last purge cycle. The titanium getter was initially melted three times to scrub any remaining oxygen in the atmosphere to limit the oxidation of the samples during melting. Samples were arc melted with a non-consumable tungsten electrode four times, flipping the ingot in between. Ingots were then washed in ethanol and ultrasonically cleaned before being mechanically broken up and remelted a further four times in the aim of complete chemical homogeneity. This was identified by Maykuth as a key step to achieving chemical homogeneity in large ingots (12).

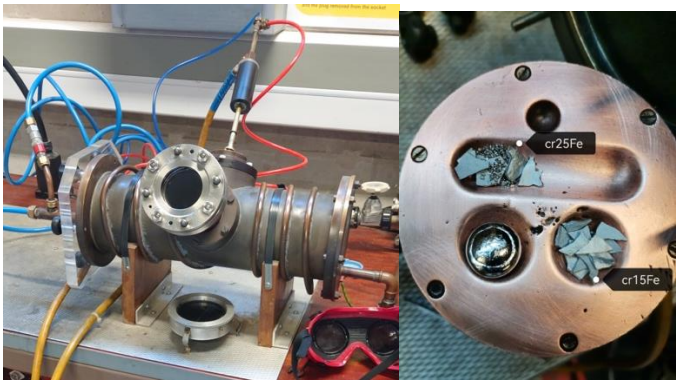


*Figure 3 - Mini arc melter (Left) and water-cooled coper hearth (right) used for melting raw elements into ingots.*

## 4.3 HEAT TREATMENT

After a further ethanol wash samples were cut (Kemet Metkon Micracut 202) to shape; wrapped in a molybdenum foil; encapsulated in a quartz tube and backfilled with argon. All samples were subjected to an initial homogenisation heat treatment of 1400$^{o}$C for 20hr. Homogenised ingots were then sectioned and samples re-encapsulated for heat treatment at 800$^{o}$C, 1000$^{o}$C and 1200$^{o}$C for 4, 20, 100 and 240 hours to allow precipitate coarsening. Encapsulated samples (Figure 4) were placed into the furnace at temperature and water quenched after the heat treatment.

*Figure 4 - Encapsulation into a quartz tube and back filled with argon.*

## 4.4 SAMPLE PREPARATION: GRINDING AND POLISHING

Samples were individually mounted (ATA OPAL 460) in conductive Bakelite then sequentially ground using SiC paper (P240 to P4000 girt) before polishing with 3 µm diamond suspension (Struers) for 15 minutes and then 0.25 µm colloidal silica OPS (MetPrep) for 1 hour with a TPOL and ethanol wash in between stages. Initial observations to check for a good polish were carried out on a Zeiss optical microscope and repolished if needed.

## 4.5 MICROSTRUCTURE CHARACTERISATION

### 4.5.1 Scanning Electron Microscope

Polished samples (Figure 5) were imaged in a Scanning Electron Microscope (SEM, JEOL 7000 and Quanta FEI-FIB, 20 keV Field Emission Gun) equipped with an Energy Dispersive X-Ray (EDX, Oxford Instruments or Brucker) detector run by Oxford Instruments Aztec or Inca software. The EDX detector provided quantitative analysis of the chemical composition of the alloys providing an average composition over 5 approximate 100x100 $\mu m^2$ areas with the exact composition provided in Table 3.

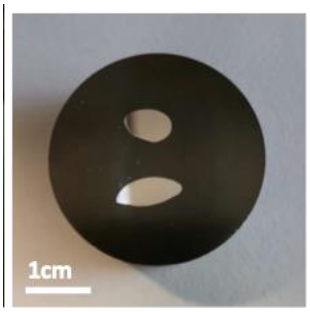


*Figure 5 - Mounted sample, polished for SEM observation*

*Table 3: EDX composition of each alloying addition. From here on samples will be referred to by their nominal compositions rather than their actual compositions.*

| | EDX Chemical Analysis at.% | | | |
|---|---|---|---|---|
| | **Cr** | **Ni** | **Al** | **Fe** |
| **Cr-5Ni-5Al** | **89.7±5** | **5.5±3** | **4.8±0.3** | **N/A** |
| **Cr-10Ni-10Al** | **79.9±0.2** | **10.7±0.3** | **9.4±0.4** | **N/A** |
| **Cr-5Ni-5Al-10Fe** | **80.8±0.1** | **4.6±0.1** | **5.1±0.1** | **9.5±0.1** |
| **Cr-10Ni-10Al-20Fe** | **59.4±0.3** | **9.8±0.2** | **10.6±0.1** | **20.3±0.1** |

### 4.5.2 Coarsening Rate

Ternary and quaternary compositions were imaged at several magnifications.

Images were processed using a machine learning algorithm within FIJI image analysis software (51) to produce an average area of each precipitate in an image. Assuming spherical precipitates due to the coherent nature and spherical appearance, the average radius was calculated. By comparing the initial (homogenised) precipitate size to the size after heat treatment, a rate in change in volume can be calculated as the coarsening rate. Samples with a low volume fraction of small precipitates could not be measured accurately on the SEM and therefore required Transition Electron Microscopy (TEM, JEOL 2100 and F20) was required to deduce the precipitate size.

TEM Samples were prepared using a dual beam gallium Focused Ion Beam (FIB, Quanta FEI-FIB) utilising mining, lift-out and thinning techniques until the sample was thin enough for electron transmission. Similar mining and thinning techniques using the FIB were also utilised to manufacture needles for Atom Probe Tomography (APT).

### 4.5.3 Atom Probe Tomography

To accurately deduce the chemical composition of the precipitate and matrix as well as the compositional change over the precipitate-matrix interface, APT was carried out using a CAMECA LEAP 5000XR in voltage mode. APT evaporates an atom at a time from the needle and by determining its time of flight and mass spectrum a 3D reconstruction of the needle can be generated. APT data was analysed using AP suite utilising proxi-grams, iso-surfaces, and regions of interest to deduce the compositional variance over a surface and the local compositions of the matrix and precipitate. The results will inform future compositions in order to specifically investigate the properties of the matrix and precipitate.

## 4.6 MECHANICAL TESTING

Hardness measurements (Mitutoyo HM-124) were taken of all samples after polishing using a 500 g load. Indentations were also imaged using the SEM to allow for future slip trace analysis for potential micro-mechanics investigations or collaborations.

## 4.7 OXIDATION EXPERIMENT IN DECHEMA

Oxidation experiments were performed on Cr-5Ni-5Al and Cr-5Ni-5Al-10Fe aged at 1200°C for 4 hours using thermogravimetric analysis (TGA) in Dechema, Frankfurt. The TGA facility comprises a precision balance (Sartorius M25D-V) and a programmable furnace (Carbolite CTE 15/75). Samples with size of ~3x3x0.3 $cm^3$ were load in an aluminide tube holder which has two holes on the bottom to allow air flow across the sample. The aluminide holder was hung into the furnace using a cage made of platinum wire covered with alumina tubes carrying the sample in synthetic air with a linear gas flow rate of 204 cm/h. Additionally, helium was used as protective gas for the balance. After stabilizing the balance in the gas flow for 4 hours, the furnace was heated to 1200°C and 1000°C with a heating rate of 15 K/min. An oxidation time of 50-100 h was chosen, after which the furnace shuts off and cools down.

# 5 RESULTS AND DISCUSSION

## 5.1 TERNARY PHASE DIAGRAM AND PHASE EVALUATION

The ternary phase diagram for Cr-Ni-Al is shown in figure Figure 6. As can be seen there is a large single phase BCC region at the homogenisation (1400ºC) temperature which shrinks to a very small region at 1000ºC.

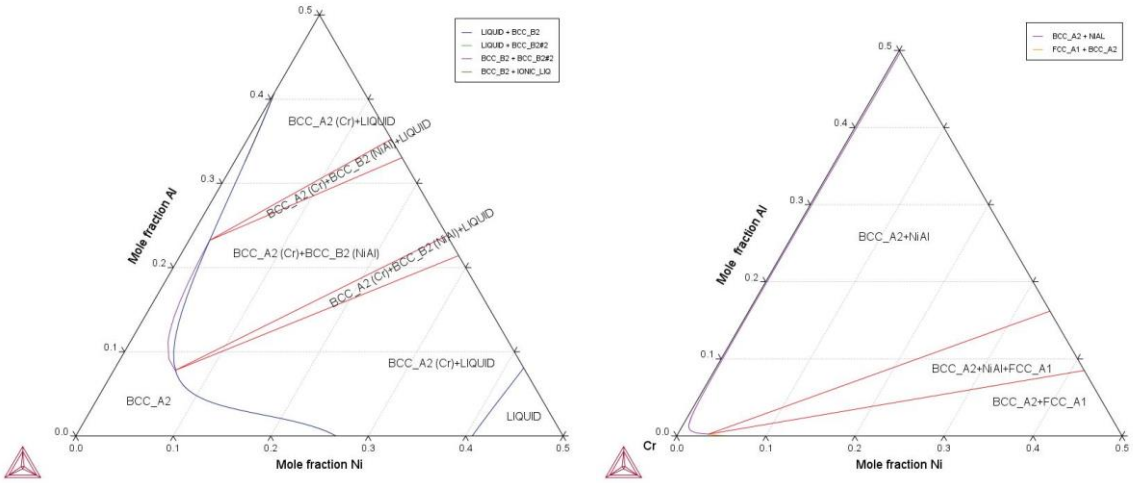


*Figure 6: Cr-Ni-Al ternary phase diagram at atmospheric pressure using the TCNI8 database (a) 1400ºC (b) 1000ºC.*

The ternary alloy Cr-5-5 after APT reconstruction can be seen if figure Figure 7. It is clear (Figure 7) that the needle has intercepted a precipitate due to the clustering of nickel and aluminium and depletion of chromium. Small amounts of iron and nitrogen are almost homogeneously present in the needle as impurities.

As predicted the phase diagrams (Figure 6) and supported by Royer, 2008 the solubility for NiAl in the chromium matrix is indeed very low even at 1000ºC (41). This is evident in the APT results indicating that <1 at.% Ni and Al are in solid solution with chromium while there is very limited chromium in the precipitate.

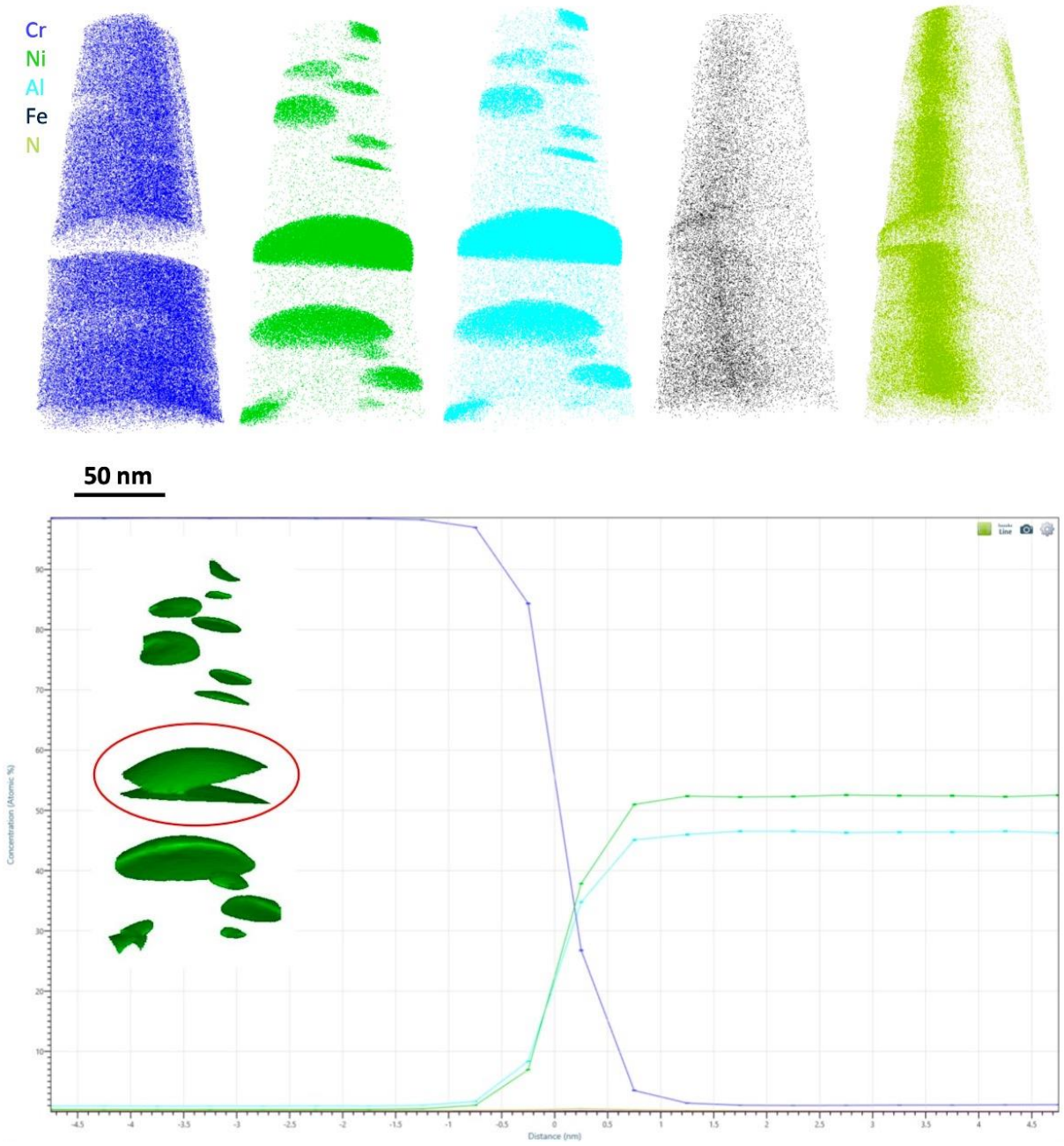


*Figure 7: Cr-5Ni-5Al APT needle reconstruction with proxigram showing compositional variance over precipitate matrix interface. Matrix composition ~98.5 at.% Cr, 1 at.% Ni, and 0.4 at.% Al. Precipitate composition ~53 at.% Ni, 46 at.% Al, and 1 at.% Cr.*

## 5.2 QUATERNARY MICROSTRUCTURE AND PHASE EVALUATION

CALPHAD investigations into the pseudo-binary Cr-NiAl-Fe phase diagram (Figure 8) identifies that the addition of iron increases the solubility of NiAl within the chromium matrix shown by an increase in solubility of NiAl from 10 at.% to almost 30 at.% by adding iron form 0 at.% to 40 at.%. Moreover, the addition of iron reduces temperature of maximum solubility from 1400$^{o}$C to 1300$^{o}$C.

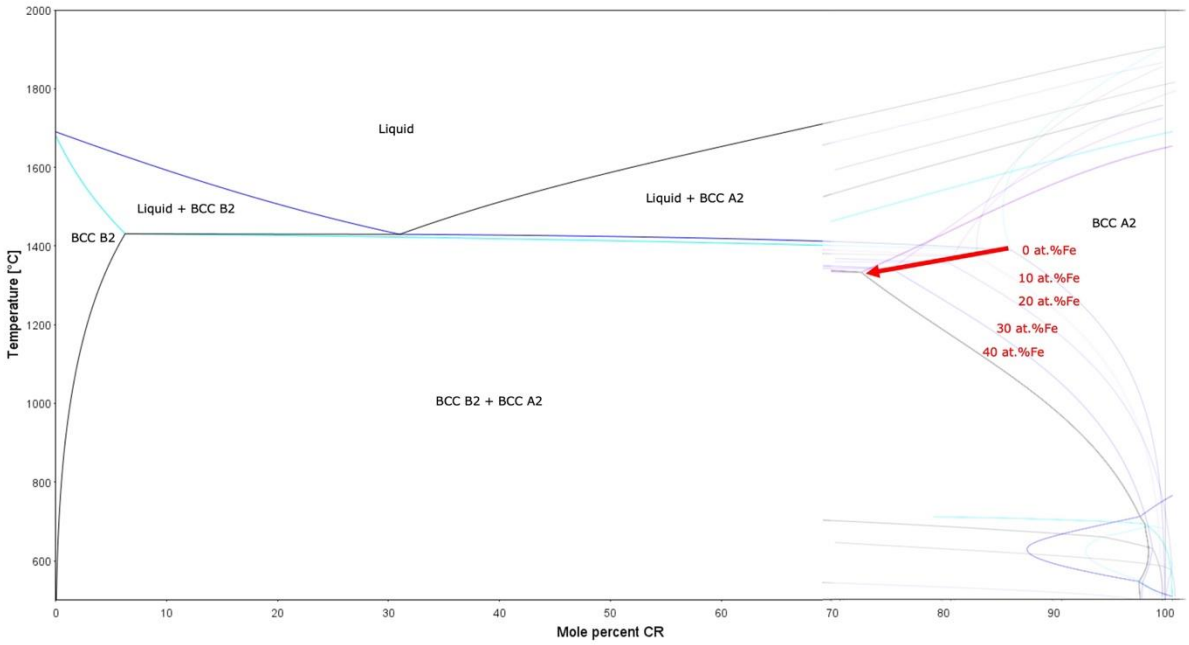


*Figure 8: Pseudo-binary phase diagram indicating the increase in predicted solubility limit for NiAl in chromium with additions of iron.*

Atom probe reconstruction (Figure 9) provides a clear visualisation of the precipitate composition within the alloy. The visualisation of the needle shows the precipitates are indeed very small (<50 nm) in diameter. It can be seen that there is limited chromium and iron in the precipitate while nickel and aluminium form the majority of the precipitate composition. It can also be seen that nitrogen and carbon impurities are also present throughout the entire tip which was likely introduced during the casting process. The proxigram (Figure 9) developed across several precipitate matrix interfaces provides the true matrix and precipitate composition. The addition of iron has also increased the nickel and aluminium content within solid solution of the chromium matrix. These compositions will be used for future alloy production to specifically analyse the properties of the matrix and precipitate.

The iron additions remain predominantly in solid solution with the chromium (shown in Figure 9) although about 4 at.% forms part of the precipitate. However, it is yet to be understood its specific role within the precipitate. Future investigations to the specific precipitate composition will help to understand this.

As can be seen in the homogenised micrographs (Figure 10), Cr-10-10 contains dendritic NiAl phase indicating that the alloy has surpassed its solubility limit leading to a non-homogeneous microstructure after homogenisation. While the alloy containing the same amount of NiAl but with 10 at.% Fe, does not exhibit the dendritic NiAl phase indicating that the solubility of NiAl has been increased with iron additions.

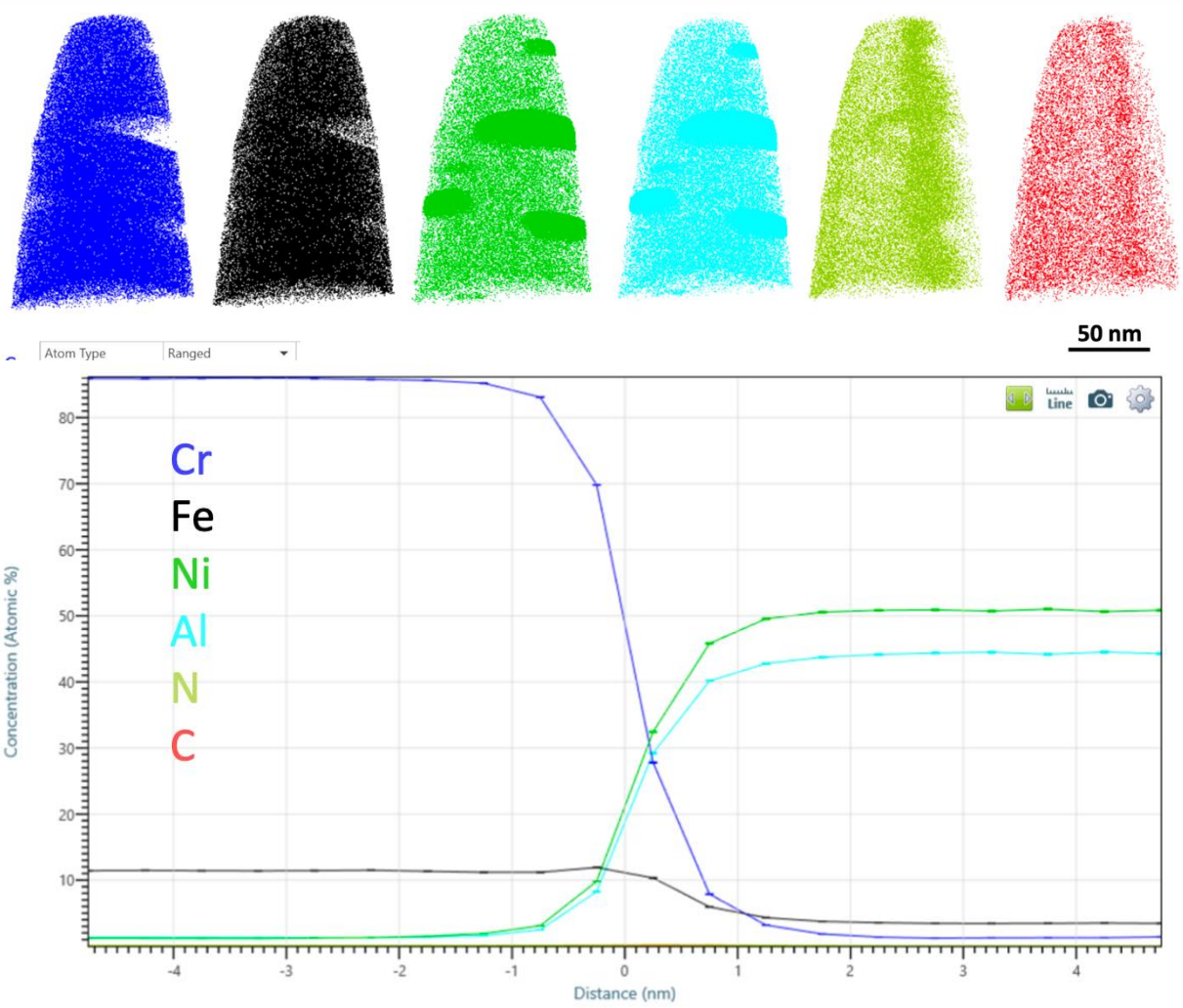


*Figure 9: Cr-5Ni-5Al-10Fe APT needle reconstruction with proxigram showing compositional variance over precipitate matrix interface. Matrix composition ~85 at.% Cr 1.5 at.% Ni 1.5 at.% Al and 12 at.% Fe. Precipitate composition ~50 at.% Ni 45 at.% Al 1 at.% Cr and 4 at.% Fe.*

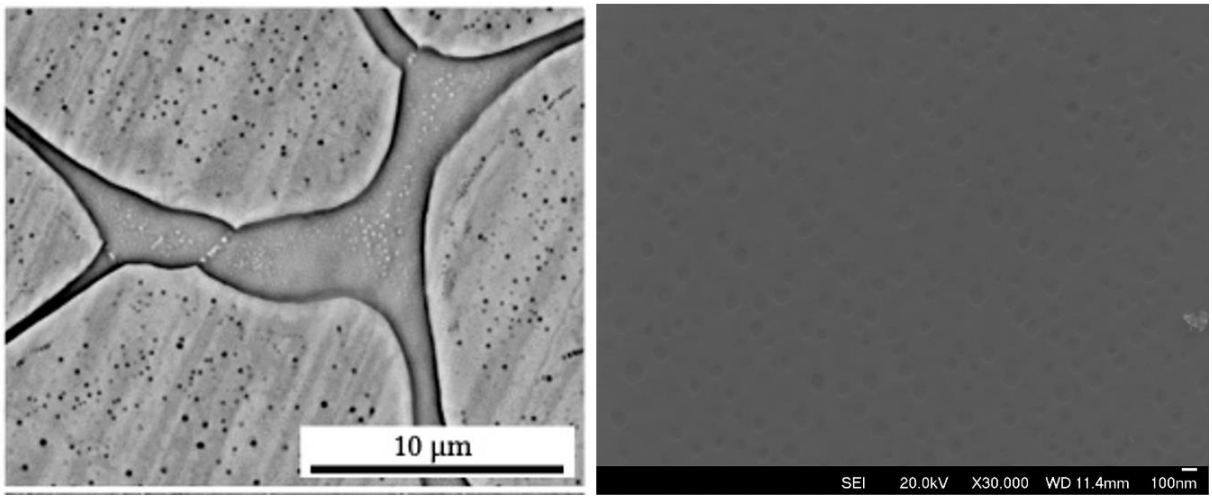


*Figure 10: Comparison of Cr-10Ni-10Al and Cr-10Ni-10Al-20Fe homogenised at 1400°C for 20 hr showing the increased solubility of NiAl with additions of iron.*

## 5.3 COARSENING RATE

Calculating the coarsening rate of the NiAl alloys utilised a machine learning algorithm summarised in Figure 11. Precipitates in TEM images (Figure 12) were manually measured due to the poor contrast between the matrix and precipitate. The distribution of precipitate radius for all images analysed resembled a normal distribution indicating an appropriate threshold and minimum precipitate area was selected. Some images with poorer contrast between the matrix and precipitate resulted in noise in the resulting analysis therefore an iterative approach to find the most appropriate minimum area had to be employed to determine a representative area fraction and average radius.

When measuring the particle sizes using TEM micrographs (Figure 12) an issue presents itself that TEM images provide the entire diameter of the precipitate due to the transmissible nature of the electrons. SEM images (Figure 11), on the other hand, provide a cross section of each precipitate that is not necessarily the full diameter. For SEM images though the average across the image makes the measured diameter representative of the precipitate although partially underestimated. Moreover, the quality of images leads to the machine learning algorithm slightly over and underestimating the area of the precipitate. While this may not cause much error for larger precipitates like those found in alloys aged at 1000 and 1200°C, it will cause a much larger error for the smaller precipitates measured at 800°C or at low ageing times.

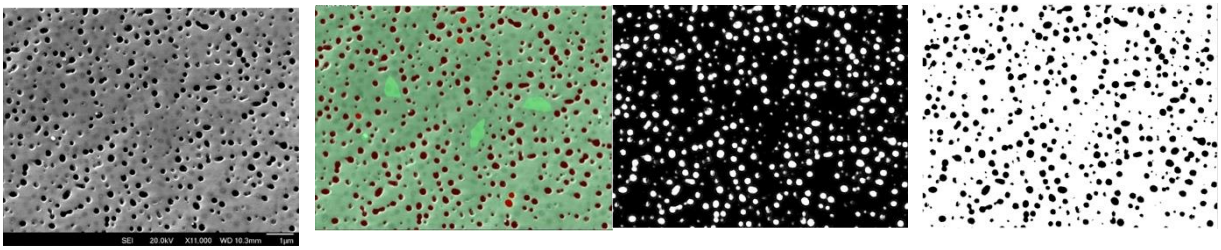

*Figure 11: Image analysis of Cr-10Ni-10Al-20Fe homogenised at 1400°C for 20 hr, water quenched then aged at 1000°C for 100 hr showing (a) Raw SEM image, (b) Weka machine learning mask, (c) Matrix overlay (d) Precipitate overlay using 14.3% threshold and a minimum precipitate area of 5000 nm$^2$.*

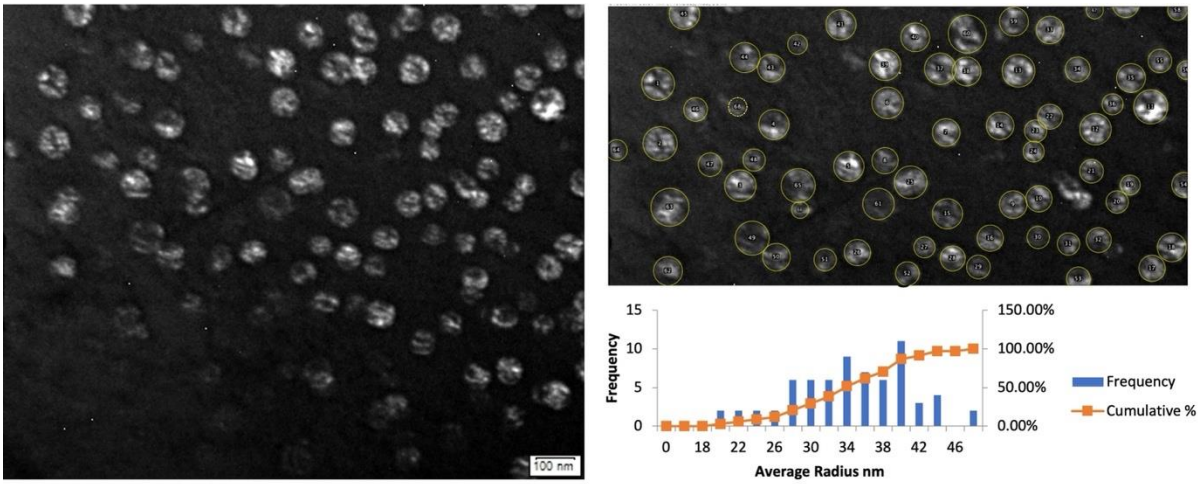


*Figure 12: Cr-5Ni-5Al homogenised at 1400°C for 20 hr. TEM image, Manual precipitate analysis, and frequency histogram. Average radius of 33 nm with a precipitate area fraction of 0.24.*

The average radius against ageing time was plotted (Figure 13) for the three ageing temperatures. Logically, ageing at 1200°C produced the largest precipitates as the higher temperature will allow for increased diffusion rates of the solute. All three temperatures resemble a cubic relationship between radius and time indicating volumetric coarsening controlled by diffusion of the solute.

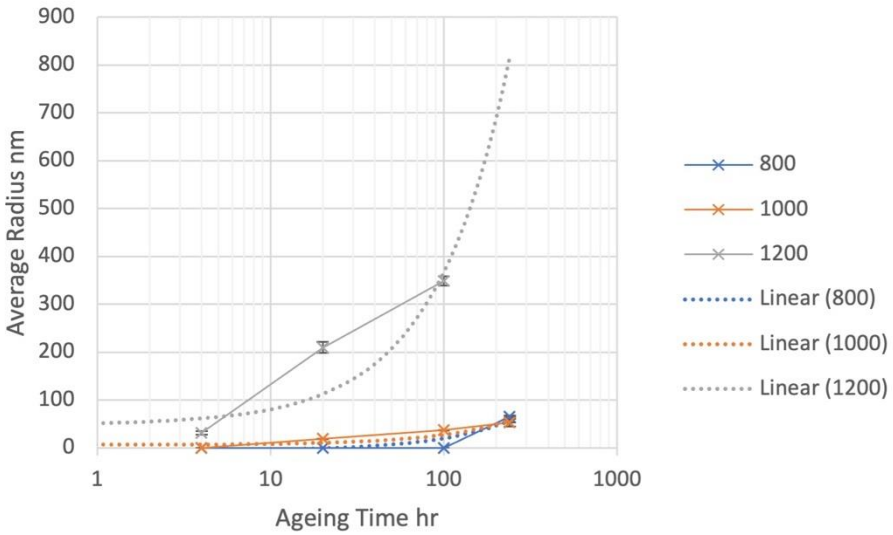


*Figure 13: Average radius against ageing time for Cr-5Ni-5Al-10Fe after homogenisation at 1400°C for 20 hr and ageing at 800, 1000 or 1200°C.*

The coarsening rate (Figure 14) at high temperatures is lower for Cr-superalloys and provides vast improvements over Ni- and Fe-superalloys. The addition of iron to the binary alloy systems further reduces the coarsening rate over the ternary alloy. The higher NiAl content of Cr-10Ni-10Al offers a reduced coarsening rate over Cr-5Ni-5Al. Low confidence can be placed on the data gathered at 800°C due to the very small size of the precipitates meaning that slight over or underestimates in the machine learning algorithm will result in a large error.

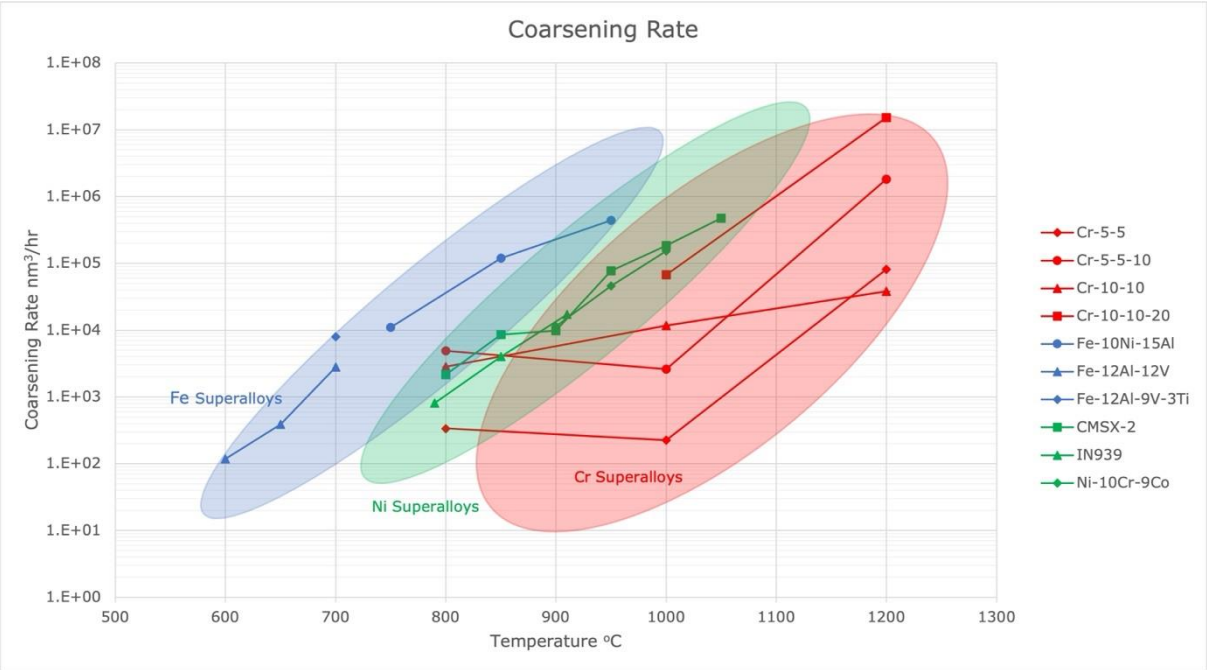


*Figure 14: Coarsening rate for Cr-superalloys (Cr-5Ni-5Al, Cr-10Ni-10Al, Cr-5Ni-5Al-10Fe, and Cr-10Ni-10Al-20Fe); Ni-superalloys (CMSX-2 Series A (35), IN939 Cast HT1 (33), Ni-10Cr-9Co (31)); and Fe-superalloys (Fe-10Ni-15Al (36), Fe-12Ni-12V (34), Fe-12Ni-9V-3Ti (32))*

## 5.4 HARDNESS OF THE SUPERALLOY

The hardness of the four alloys is presented in Figure 15. Ternary alloy systems show age softening at all ageing times and temperatures. After ageing, Cr-5Ni-5Al at 800°C negligible age softening or hardening occurs while ageing the same alloy at 1000°C results in significant age softening with a reduction of approximately 200 HV points after ageing for 240 hours.

Similarly, the hardness of Cr-10Ni-10Al follows an age softening effect with a relatively stable hardness after ageing at 800°C and significant softening at 1000°C. The average hardness remains similar to Cr-5Ni-5Al.

As for the addition of iron to the ternary systems, the initial homogenised hardness increases by approximately 100 HV points when compared to the equivalent ternary system. The addition of iron also stabilises the hardness after ageing with limited age softening occurring in both systems.

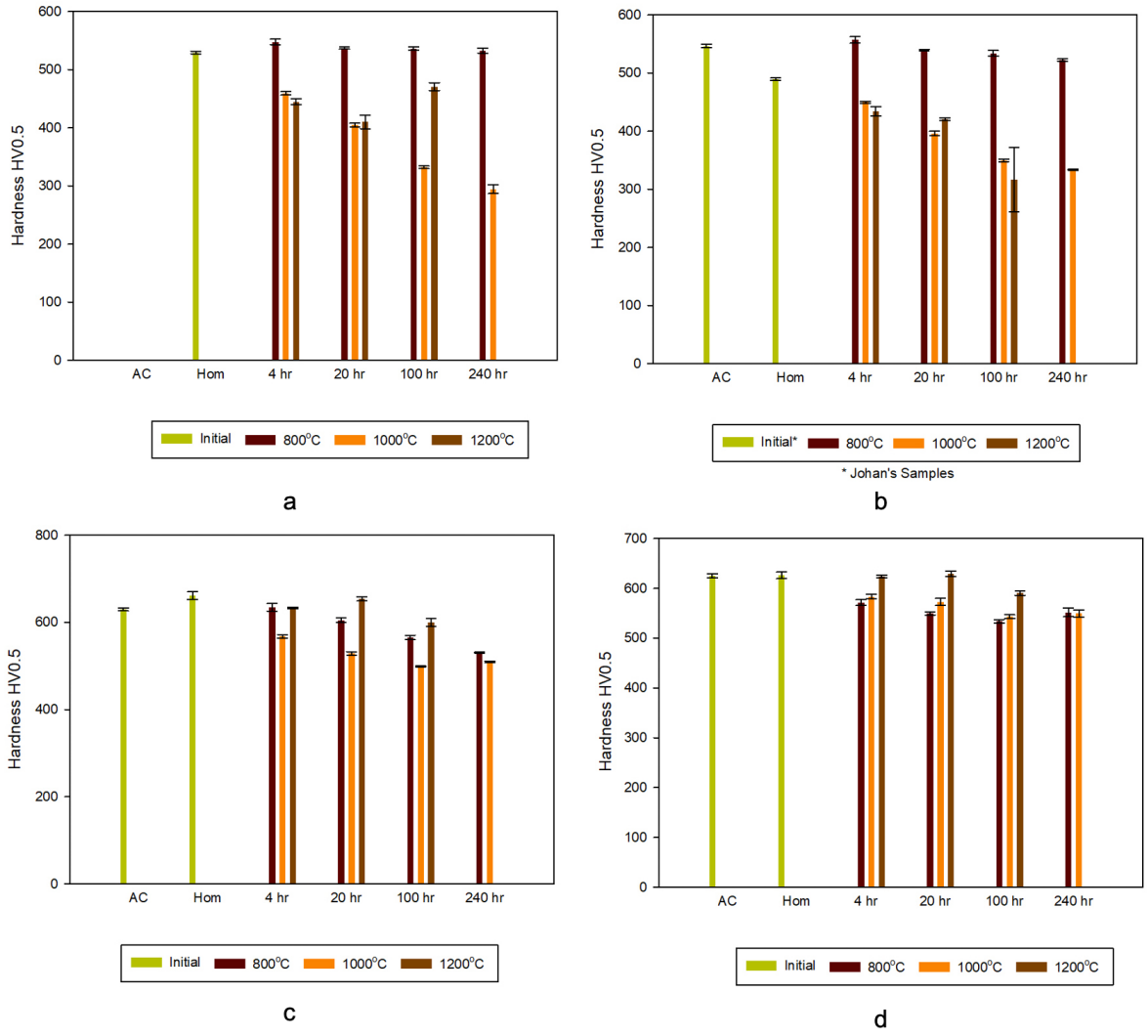


*Figure 15: Hardness plots against ageing time for (a) Cr-5Ni-5Al, (b) Cr-10Ni-10Al (as cast and homogenised from (42)), (c) Cr-5Ni-5Al-10Fe, and (d) Cr-10Ni-10Al-20Fe.*

## 5.5 OXIDATION KINETICS

Cr-NiAl(-Fe) alloys show improved oxidation resistance compared to Cr but exhibit similar oxidation kinetics. At 1200°C there is a paralinear mass gain and the typical mass discontinuities (typical for Cr-based alloys). However, the parabolic mass gain is rather high in the beginning. It seems as at first a mixed oxide or a Ni- containing oxide formed and later a more protective Cr-rich oxide formed. At 1000°C no paralinear kinetics as there is rather a linear mass gain instead of a linear mass loss. The oxide scale has to be further analysed for a deeper conclusion and oxidation resistance needs to be improved such as adding Si as demonstrated in Cr-$Cr_3Si$ alloys (52).

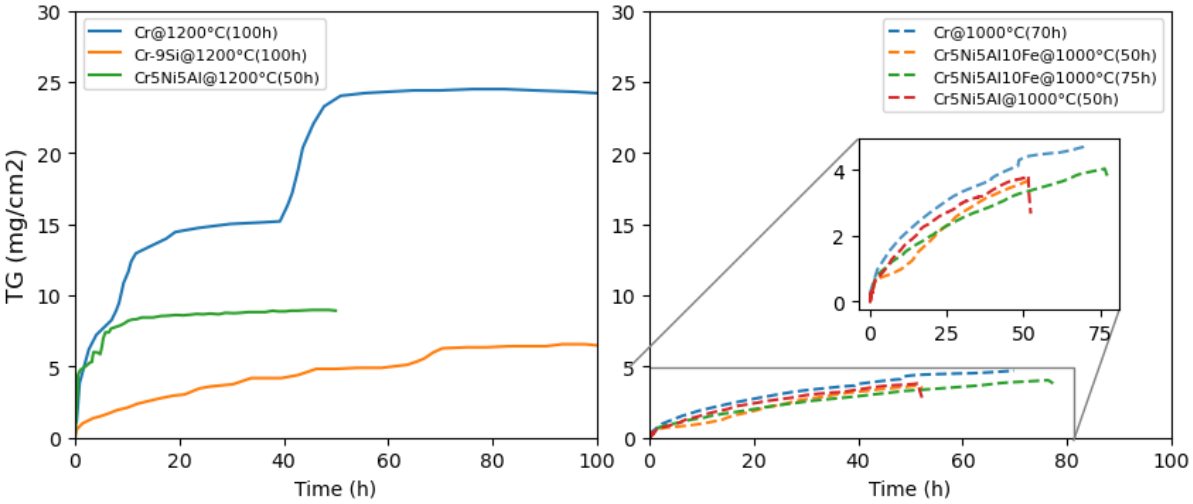


*Figure 16 Thermogravimetric (TG) measurements of the alloys and of pure Cr (52,53), Cr-Cr3Si alloy (52), Cr-5Ni-5Al and Cr-5Ni-5Al-10Fe.*

# 6 CONCLUSIONS

After investigating the solubilities, coarsening rates and hardness of ternary and quaternary Cr-NiAl(-Fe) systems the following conclusions were established:

- The design of Cr-NiAl alloys with iron additions is validated by CALPHAD calculation and experiment. The addition of iron increases the solubility of the NiAl phase which avoids the dendritic and eutectic precipitates and allows a higher volume fraction of precipitate compared to the ternary alloys.
- Cr-NiAl has an improved coarsening resistance over ferritic superalloys and Ni-superalloys at high temperatures. The presence of NiAl precipitate leads to substantial precipitate strengthening over pure chromium.
- Iron increases the solubility of nickel and aluminium in solid solution with chromium. Iron, nickel and aluminium in solid solution with chromium increases the hardness of the matrix by solid solution strengthening.
- Cr-NiAl alloys show improved oxidation resistance compared to pure Cr but bear similar oxidation kinetics. Iron addition show minor effect on the oxidation kinetics of Cr-NiAl.

# 7 FUTURE WORK

Future work will focus on several aspects:

- Concurrent investigations into additions of other minor additions like Co, Ti, Ag and V will be carried out to deduce what affect they may have on improving the ductility of the chromium superalloys (54, 55). These investigations will follow similar testing programmes to feed into the widening knowledge base of chromium alloy systems suitable for high temperature environments.
- Oxidation experiment and oxide scale analysis of Cr-NiAl will be performed with **Dechema** to obtain inside into the oxidation kinetics of Cr-NiAl alloys to provide further pathway for the improvement of their oxidation resistance.

- The mechanical properties of various Cr-NiAl compositions comparing them to pure chromium and binary alloys will be determined in **Dechema** and **CIEMAT**. Initially this will consist of hot compression tests in Dechema to screen brittle-ductile behaviour of samples. Small punch testing will then be carried out at a range of temperatures from -150ºC to 800ºC to determine the strength and creep resistance of Cr-NiAl alloys. Results obtained from the small punch testing will inform which samples will then be further tested via small punch creep to determine the material suitability at high temperatures (>500°C) and pressures over the expected 20 year service life.
- The mechanical properties of Cr-NiAl will be compared with the state-of-the-art materials (Ni superalloys and austenitic steels) characterised and tested using the same facility in **CIEMAT** and **OCAS**.
- The understanding of thermophysical properties of Cr-NiAl will be achieved by the modelling in **VTT**. Experiment data (coarsening rate, EBSD, strain-stress behaviour etc.) will be used as input parameters for simulation to obtain insight into the deformation mechanisms in these alloys and better predict their long-term behaviour.
- Under the organisation of **DLR**, Cr-NiAl samples with different geometries will be manufactured and delivered to work package 4 (**CIEMAT**, **CVR**, **Julich)** for CSP environment testing including wear test using ceramic particles, long-term oxidation, CO2 and s-CO2 exposure.

# 8 REFERENCES

1. Stephens JR, Klopp WD. Ductility mechanisms and superplasticity in chromium alloys. 1968;34.

2. Klopp WD. Recent Developments in Chromium and Chromium Alloys. JOM J Miner Met Mater Soc. 1969 Nov;21(11):23–32.

3. Naka S, Thomas M, Khan T. Potential and prospects of some intermetallic compounds for structural applications. Mater Sci Technol. 1992 Apr;8(4):291–8.

4. Naka S, Khan T. Alloy Design. In: Intermetallic Compounds - Principles and Practice [Internet]. John Wiley & Sons, Ltd; 2002 [cited 2022 May 30]. p. 841–55. Available from: https://onlinelibrary.wiley.com/doi/abs/10.1002/0470845856.ch41

5. HM Treasury. Net Zero Review: Analysis exploring the key issues. 2021.

6. CSP: Simple solutions for generating heat [Internet]. [cited 2022 Jun 24]. Available from: https://www.eni.com/en-IT/operations/concentrated-solar-power.html

7. Office EP. COMPONENTS' AND MATERIALS' PERFORMANCE FOR ADVANCED SOLAR SUPERCITICAL CO2 POWERPLANTS | COMPASsCO2 Project | Fact Sheet | H2020 | CORDIS | European Commission [Internet]. 2022 [cited 2022 Jun 1]. Available from: https://cordis.europa.eu/project/id/958418

8. Ro Y, Koizumi Y, Nakazawa S, Kobayashi T, Bannai E, Harada H. Development of Cr-base alloys and their compressive properties. Scr Mater. 2002 Mar 11;46(5):331–5.

9. Harada Y, Ohmori M. Ductile–Brittle transition behavior of rolled chromium. J Mater Process Technol. 2004 Nov;153–154:93–9.

10. Murdock H. Processing effects on the ductility of chromium-vanadium alloys. 2010.

11. Terentyev D, Khvan T, You JH, Van Steenberge N. Development of chromium and chromium-tungsten alloy for the plasma facing components: Application of vacuum arc melting techniques. J Nucl Mater. 2020 Aug;536:152204.

12. Maykuth DJ, Gilbert A. Chromium and Chromium Alloys. Defense Metals Information Center, Battelle Memorial Institute; 1966.

13. Bergman TL, Lavine AS, Incropera FP, DeWitt DP. Introduction to heat transfer. John Wiley & Sons; 2011.

14. Sciences A. Melting Points of Elements Reference [Internet]. [cited 2022 Jun 24]. Available from: https://www.angstromsciences.com/melting-points-of-elements-reference

15. Density of Elements Chart – Angstrom Sciences Elements Density Table [Internet]. [cited 2022 Jun 24]. Available from: https://www.angstromsciences.com/density-elements-chart

16. Du Y, Tan Z, Yang Y, Wang X, Zhou Y, Li J, et al. Creep Properties of a Nickel-Based Single Crystal Superalloy with Low Density. Met Mater Int. 2021 Dec 1;27(12):5173–8.

17. Ramsperger M, Singer RF, Körner C. Microstructure of the Nickel-Base Superalloy CMSX-4 Fabricated by Selective Electron Beam Melting. Metall Mater Trans A. 2016 Mar;47(3):1469–80.

18. Matsushita T, Fecht HJ, Wunderlich RK, Egry I, Seetharaman S. Studies of the thermophysical properties of commercial CMSX-4 alloy. J Chem Eng Data. 2009;54(9):2584–92.

19. Matsumoto Y, Oki K, Tanaka M, Fujigami F, Harada Y, Morinaga M. Room-temperature ductility and surface notch sensitivity of chromium alloyed with vanadium and molybdenum. Mater Sci Eng A. 2004 Nov;385(1):133–9.

20. Taneichi K, Narushima T, Iguchi Y, Ouchi C. Oxidation or Nitridation Behavior of Pure Chromium and Chromium Alloys Containing 10 mass%Ni or Fe in Atmospheric Heating. Mater Trans. 2006;47(10):2540–6.

21. Garrod RI, Wain HL. Dislocation arrangements and brittleness in chromium. J Common Met. 1965 Aug;9(2):81–94.

22. Gilbert A, Allen BC, Reid CN, Gilbert A, Allen BC, Reid CN. An Investigation of Mechanical Properties of Chromium, Chromium-Rhenium, and Derived Alloys. 1964.

23. Klopp WD. A review of chromium, molybdenum, and tungsten alloys. J Common Met. 1975 Oct 1;42(3):261–78.

24. Gu YF, Harada H, Ro Y. Chromium and chromium-based alloys: Problems and possibilities for high-temperature service. JOM J Miner Met Mater Soc. 2004 Sep 1;56(9):28–33.

25. Kanou G, Harima N, Takaki S, Abiko K. Mechanical Properties of a High-Purity 60 mass%Cr–Fe Alloy. Mater Trans JIM. 2000;41(1):197–202.

26. Abiko K. Why Do We Study Ultra-High Purity Base Metals? Mater Trans JIM. 2000;41(1):233–7.

27. Abiko K, Kato Y. Properties of a High-Purity Fe–Mass% Cr Alloy. Phys Status Solidi A. 1998;167(2):449–61.

28. Asahina M, Harima N, Takaki S, Abiko K. High-Temperature Mechanical Properties of High-Purity 70 mass% Cr–Fe Alloy. Phys Status Solidi A. 2002;189(1):87–96.

29. Vo NQ, Liebscher CH, Rawlings MJS, Asta M, Dunand DC. Creep properties and microstructure of a precipitation-strengthened ferritic Fe–Al–Ni–Cr alloy. Acta Mater. 2014 Jun;71:89–99.

30. Ulrich AS, Pfizenmaier P, Solimani A, Glatzel U, Galetz MC. Improving the oxidation resistance of Cr-Si-based alloys by ternary alloying. Corros Sci. 2020;165:108376.

31. Zhang J, Liu L, Huang T, Chen J, Cao K, Liu X, et al. Coarsening kinetics of γ′ precipitates in a Re-containing Ni-based single crystal superalloy during long-term aging. J Mater Sci Technol. 2021;62:1–10.

32. Ferreirós PA, Alonso PR, Rubiolo GH. Effect of Ti additions on phase transitions, lattice misfit, coarsening, and hardening mechanisms in a Fe2AlV-strengthened ferritic alloy. J Alloys Compd. 2019 Oct 25;806:683–97.

33. Jahangiri MR, Arabi H, Boutorabi SMA. Comparison of microstructural stability of IN939 superalloy with two different manufacturing routes during long-time aging. Trans Nonferrous Met Soc China. 2014 Jun 1;24(6):1717–29.

34. Ferreirós PA, Alonso PR, Rubiolo GH. Coarsening process and precipitation hardening in Fe2AlV-strengthened ferritic Fe76Al12V12 alloy. Mater Sci Eng A. 2017 Jan;684:394–405.

35. Ges A, Fornaro O, Palacio H. Coarsening behaviour of a Ni-base superalloy under different heat treatment conditions. Mater Sci Eng -Struct Mater Prop Microstruct Process - MATER SCI ENG -STRUCT MATER. 2007 Jun 1;458:96–100.

36. Rosales-Dorantes HJ, Cayetano-Castro N, Lopez-Hirata VM, Saucedo-Muñoz ML, Villegas-Cardenas D, Hernández-Santiago F. Coarsening process of coherent β′ precipitates in Fe–10 wt-%Ni–15 wt-%Al and Fe–10 wt-%Ni–15 wt-%Al–1 wt-%Cu alloys. Mater Sci Technol. 2013 Dec 1;29(12):1492–8.

37. Murray JL. The Al-Cr (aluminum-chromium) system. J Phase Equilibria. 1998 Aug;19(4):368.

38. Locq D, Caron P, Ramusat C, Mévrel R. Chromium-Based Alloys Strengthened by Ordered Phase Precipitation for Gas Turbine Applications. Adv Mater Res. 2011;278:569–74.

39. Doğan ÖN, Song X, Chen S, Gao MC. Microstructural study of high-temperature Cr–Ni–Al–Ti alloys supported by first-principles calculations. Intermetallics. 2013 Apr;35:33–40.

40. McKeehan LW. The Crystal Structure of Iron-Nickel Alloys. Phys Rev. 1923 Apr 1;21(4):402–7.

41. Royer L, Mathieu S, Liebaut C, Steinmetz P. Study of the Microstructure and Oxidation Behavior of Chromium Base Alloys Strengthened by NiAl Precipitates. Mater Sci Forum. 2008;595–598:117–25.

42. Magnussen JP. Development of Iron and Chromium Based Alloys Using the Ferritic (BCC) Superalloy Approach. 2019.

43. Wolff-Goodrich S, Marshal A, Pradeep KG, Dehm G, Schneider JM, Liebscher CH. Combinatorial exploration of B2/L21 precipitation strengthened AlCrFeNiTi compositionally complex alloys. J Alloys Compd. 2021;853:156111.

44. Asahina M, Harima N, Takaki S, Abiko K. High-Temperature Mechanical Properties of a High-Purity Cr–Ni Alloy. Mater Trans JIM. 2000;41(1):178–83.

45. Takeyama M, Liu CT. Microstructure and mechanical properties of Laves-phase alloys based on Cr2Nb. Mater Sci Eng A. 1991 Feb;132:61–6.

46. Ulrich AS, Pfizenmaier P, Solimani A, Glatzel U, Galetz MC. Strengthened Cr-Si-base alloys for high temperature applications. Int J Refract Met Hard Mater. 2018 Nov;76:72–81.

47. Pfizenmaier P, Ulrich AS, Galetz MC, Glatzel U. Determination of heat treatment parameters by experiments and CALPHAD for precipitate hardening of Cr-Alloys with Si, Ge and Mo. Intermetallics. 2020 Jan;116:106636.

48. Filippi AM. DEVELOPMENT OF DUCTILE HIGH STRENGTH CHROMIUM ALLOYS. 1970 p. 115.

49. Miracle DB, Russell S, Law CC. Slip System Modification in NiAl. MRS Online Proc Libr. 1988;133(1):225.

50. Lu Y, Zhang YH, Ma E, Han WZ. Relative mobility of screw versus edge dislocations controls the ductile-to-brittle transition in metals. Proc Natl Acad Sci. 2021 Sep;118(37):e2110596118.

51. Arganda-Carreras I, Kaynig V, Rueden C, Eliceiri KW, Schindelin J, Cardona A, et al. Trainable Weka Segmentation: a machine learning tool for microscopy pixel classification. Bioinformatics. 2017 Aug 1;33(15):2424–6.

52. Ulrich AS, Pfizenmaier P, Solimani A, Glatzel U, Galetz MC. Improving the oxidation resistance of Cr-Si-based alloys by ternary alloying. Corros Sci. 2020 avril;165:108376.

53. Lillerud K, Kofstad P. On high temperature oxidation of chromium: I. Oxidation of annealed, thermally etched chromium at 800–1100 C. J Electrochem Soc. 1980;127(11):2397.

54. Gao MC, Doğan ÖN, King P, Rollett AD, Widom M. The first-principles design of ductile refractory alloys. Jom. 2008;60(7):61–5.

55. Gu YF, Ro Y, Harada H. Tensile properties of chromium alloyed with silver. Metall Mater Trans A. 2004 Oct 1;35(10):3329–31.